EXPERIMENTAL INVESTIGATION OF FORCED-CONVECTION HEAT TRANSFER IN A WAVY CHANNEL BY DIGITAL SPECKLE PHOTOGRAPHY

Luigi Colombo, Adriano Muzzio, Alfonso Niro

Dipartimento di Energetica, Politecnico di Milano, I-20133 Milano, Italy

ABSTRACT

The paper presents experimental data on local and average heat-transfer coefficients as well as on pressure drops of air-flows through a wavy channel for Reynolds numbers ranging between 480 and 6300. The channel has a rectangular cross-section, 200 mm in width and 10 mm in height; waviness are characterized by a triangular profile and they are arranged perpendicularly to streamwise direction. Local heat transfer characteristics are investigated by non-intrusive measurements of velocity and temperature-gradient fields by means of LDV and digital speckle photography, respectively. Experimental results presented here are for fixed temperature conditions; they show that waviness significantly alters the streamwise distribution of the local Nusselt number but the per-module average increase is quite lower; the average Nusselt number over the entire channel is 60% larger with respect to the plain-channel value in laminar flow-regime while becoming a quickly increasing function of the Reynolds number as flow-regime becomes transitional (Re≈1300); at Re=6300 the enhancement factor comes up to 4. However, heat transfer augmentation is greatly penalized by the accompanying increase of the apparent friction factor which is 2÷3 times the plain-channel value in laminar flow, and up to 7 times in turbulent flow.

INTRODUCTION

Wavy-fins are an efficient and cost-effective solution to enhance heat transfer of air-flows inside compact plain-fin heat-exchangers. In fact, due to small passages and relatively low air velocity, flow is laminar or weakly turbulent and convective coefficient is low. Specially configured fin-surfaces, such as offset-strip-, louvered-, perforated-, and wavy-fins, are widely used because they provide quite larger heat-transfer rates. This performance improvement is essentially due to the alteration of duct fluid-dynamic rather than to the increase of heat-transfer-surface area. Many enhancement mechanisms can be used but those most frequently employed are periodic deflection of streamlines, periodic interruptions of the boundary layer growth and flow destabilization. Furthermore, these specially configured fin-surfaces also promote turbulence development, as the corrugation size is close to that of the fluid dynamic structures to be excited (the lower the Reynolds number, the larger these structures). Because of the large variety of possible shapes and geometries, there is a large number of studies in the open literature. For instance, Webb [1] reports more than 35 papers and almost as many are cited by Fiebig [2]. For offset strip fin geometry, correlations for predicting the Colburn and friction factors were proposed by Kays [3], Joshi and Webb [4], and Wieting [5]; similar correlations were developed by Davenport [6] for louvered fin geometry. Finally, wavy fin geometry is also the subject of some interesting studies, such as those by Goldstein and Sparrow [7], and Ali and Ramadhyani [8], but there are not quite general correlations for this geometry because of a rather lacking database. For these motivations, we are currently performing an experimental and numerical investigation on flows through channels with wavy walls.

This paper reports on local and average heat transfer characteristics as well as on pressure drops of air-flows through a wavy channel at Reynolds numbers within the typical operating range of plain-fin heat-exchangers. Waviness have a triangular cross-section (an apex on a wall coincides with a trough on the other one) which induce a periodic streamline deflection.

EXPERIMENTAL EQUIPMENT AND METHODS

The experimental setup is composed by the air circuit, containing the test channel, and by the heating water circuit. The test channel has a rectangular cross section of 200 mm in width and 10 mm in height, it is horizontally positioned and is constituted by entry, test and exit sections. Room air flows into the entry section through an opening with rounded surfaces; the entry section is a 1 m long, that is about 55 times the hydraulic diameter, and its walls are not heated; at the end of this section, fully developed flow conditions are attained. The test section is 800 mm long with glass side-wall. The top and bottom walls are made with aluminum-alloy blocks, strongly tightened between them and to their own heating water channel. To monitor the wall temperatures of the test-section, six thermocouples are inserted into the lower wall, and two into the upper one; the thermocouple tips are placed 0.5 mm beneath the channel surface. Downstream the test section, there are a 0.5-m-long exit-section, a filter, three float-type flowmeters (nominal accuracy of 2%), a metering valve and a blower operating in suction mode. Eventually, the exhausted air is discharged outside the laboratory. The heating water circuit is mainly composed by a heat bath, which provides a high mass flow rate of water at a temperature constant within 0.1 K, and by the channels mounted on the lower and upper walls of the test section; water flows in opposite direction of the air.

Wall-temperature difference is about 0.1 K in perpendicular-direction to air-flow, and 0.8 K in parallel-direction.

Air temperature is measured at the test-section entrance, and upstream and downstream the flow-meters. The x-direction component of the air velocity is measured by means of the laser Doppler velocimetry, whereas we used double-exposure digital speckle photography to investigate the local heat fluxes. This is an optical technique which enables the non-intrusive measurement, in transparent media, of refractive index gradients by evaluating speckle displacements between the object exposure and a reference exposure, as described by Fomin in [9]. By such information, using the proper physical laws, we can reconstruct the temperature gradient field and, thus, the local heat fluxes. For the aims of this work, a "subjective speckles" record system, i.e., where speckle patterns are generated by an optical system, is shown to provide higher spatial resolution and wider measurement range, as discussed by Jones and Wykes in [10]; finally, the digital recording, as by a CCD camera, makes very easy both data storage and processing.

Classical optical schemes for speckle photography of transparent media are reported by Fomin [9]; this reference also shows the experimental set-up configuration should be determined by trade-off between the area of spatial averaging of data on the image plane and sensitivity, i.e., the speckle-shift to ray-deflection-angle ratio. For the present applications, typical values of the ray-deflection angle are in order of magnitude of about 1 mrad. To convert such a deflection into a speckle displacement of at least 5 pixels on the image plane, a sensitivity of 40 mm/rad is required. Moreover, the spatial averaging area can be assumed small enough with respect to the test-section dimensions, if its equivalent diameter d_0 is of 0.5 mm. To meet these requirements, the scheme of the optical probe shown in Figure 1 has been adopted. The lenses L_1 and L_2 are actually two couples of achromatic doublets to ensure the best coupling of the conjugated planes, as discussed by Curotti [11]. Table 1 reports diameters and focal lengths of the doublets used. In such a scheme, assuming a refractive-index constant in z-direction, i.e., perpendicular to the channel axis, and parabolic ray paths, the speckle displacement $\vec{S}$ is correlated to the refractive-index gradient as follows

$$\vec{S} = \frac{L}{n_0} \cdot \frac{M_2 M_3}{M_1} d \cdot \vec{\nabla} n \tag{1}$$

where L is the test-section length in z-direction, n_0 the refractive index in the reference state, M_i the magnification of i-th lens, and d the defocusing distance. Finally, using the Gladstone-Dale Equation, the speckle displacement can be correlated to the temperature gradient

$$\vec{S} = \frac{3}{2} \cdot \frac{p\bar{r}}{RT^2} \cdot \frac{L}{n_0} \cdot \frac{M_2 M_3}{M_1} d \cdot \vec{\nabla} T \tag{2}$$

where p is the absolute pressure, R the universal constant of gases, and $\bar{r}$ the molar refractivity. Furthermore, the sensitivity K is

Doublet	Diameter a [mm]	Focal length f [mm]
$L_{1,1}$ and $L_{1,2}$	25.4	150.0
$L_{2,1}$ and $L_{2,2}$	12.7	50.8
L_3	12.7	19.0

Table 1. Diameters and focal lengths of lenses.

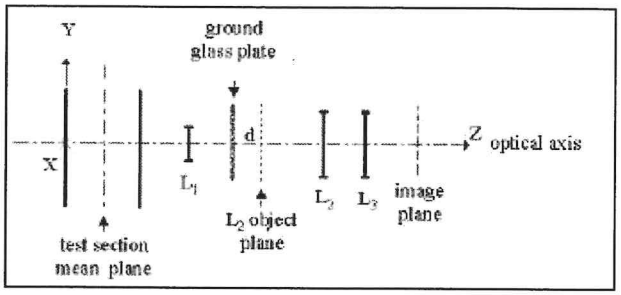

Figure 1. Scheme of the optical probe.

$$K = \frac{M_2 M_3}{M_1} d \tag{3}$$

whereas the diameter of the spatial averaging area can be estimated by methods of geometrical optic [9] as

$$d_o = \frac{a_2 d}{f_2} \frac{M_2}{M_2 + 1} \tag{4}$$

The condition d_0=0.5 mm is satisfied by setting d=4 mm without any magnification (M_2=1). The lens L3 provides magnification to achieve the desired sensitivity (M_3=10). Accuracy for d is about ±0.5%, and ±1.5% for M_3.

Speckle patterns are electronically recorded by a monochrome, progressive-scan, ½-CCD camera with 760×530 pixel resolution, 10 bit dynamic range, and 25 not-interlaced frames per second. Since the test-section area captured by the camera, positioned in the optical probe, is only 640 μm × 446 μm, a test-section scanning is needed. Thus, the optical probe is mounted on a shifting system which allows horizontal and vertical movement within 5-μm accuracy.

The speckle displacement has been determined seeking the position of the maximum of the cross-correlation function

$$C(m^*, n^*) = \frac{1}{m \cdot n} \sum_{i=1}^{m} \sum_{j=1}^{n} \left[g(i,j) g'(i+m^*, j+n^*) \right] \tag{5}$$

where g(i,j) and g'(i,j) are the luminous intensities at the pixel location (i,j) of the speckle patterns recorded in the reference state and in the operating conditions, respectively. Cross-correlation has been calculated on five consecutive sub-domains of the recorded frames, 106×106 pixel large, centered on the mean line. This dimension is about ten times greater than the maximum value of the speckle displacement occurred; hence, it is large enough to avoid excessive speckle-pattern decorrelation due to displacement itself, which causes some speckle to cross the calculation domain boundaries.

The actual similarity of the compared images is assessed by evaluating the so-called correlation degree defined as follows:

$$\zeta = \frac{\max(C)}{\sqrt{\max(A_1) \cdot \max(A_2)}} \leq 1 \tag{6}$$

where A_1 and A_2 auto-correlations of the speckle patterns to be compared. Obviously, $\zeta = 1$ only if images are identical.

In addition to local thermal fields, average heat transfer characteristics over the entire channel were also investigated by measuring the air bulk-temperature at the outlet of the test-

section. This measurement was performed equipping the exit section with two rows of turbolizers and with a convergent channel; this conveys the air flow into a narrow duct (1 cm in width) which is filled with a tangle of copper fine wires with two thermocouples fitted in. The temperature measurement accuracy is of 0.2 K. The average Nusselt number over the channel is evaluated as

$$Nu_{av} = \frac{\rho V c_p D_h}{k A_s} \ln(\theta_i / \theta_o) \qquad (7)$$

where V is the volume flow rate of air, ρ the density evaluated at the temperature and pressure where V is measured, c_p the specific heat at constant pressure, k the thermal conductivity, A_s the total area of the heated surface, θ_i and θ_o are the wall to air-bulk-temperature difference at the entrance and the exit of the channel, respectively. The uncertainty on Nu_{av} measurement, evaluated by a propagation error analysis, is 6% on the average but it becomes larger than 15% when θ_o lowers under 2 °C, namely, at the highest values of Nu_{av}. Finally, pressure drop is measured by means of two probes, each consisting of a 6-mm o.d. tube with two pairs of 0.1-mm-diameter pressure taps on the tip, plugged into the channel; these probes are connected to a differential micromanometer with a 0.125-Pa sensitivity. The apparent Darcy friction factor is calculated as

$$f = \frac{2 D_h A^2}{\rho V^2} \frac{\Delta p}{L_{chan}} \qquad (8)$$

where Δp is the pressure drop over the entire wavy channel, A and L_{chan} are the cross section area and the length of the channel, respectively. The measurement of this factor is affected by an uncertainty of 5.2% on the average but this comes up to 10% at the lowest values of Δp.

EXPERIMENTAL RESULTS

The channel investigated in this paper is schematically shown in Figure 2, whereas Table 2 lists its main geometric characteristics. Heat transfer data are obtained keeping the lower and upper walls at the uniform temperature of 50 °C, whereas the measurements of velocity and pressure drop of the air flow are performed with channel walls at room temperature because the thermal effects on fluid dynamic are negligible under this temperature difference. In all the tests, air inlet temperature is about 20 °C. The measurement region lies at the thirteenth corrugation of the lower wall, 250 mm downstream of the test section inlet, where previous investigations by the authors in [12] have assessed the attainment of periodically fully developed flow conditions. Temperature-gradient measurements are taken along six vertical lines, as depicted in Figure 3, at 12 locations equally spaced 0.9 mm; if needed, close to the boundaries, spacing is halved.

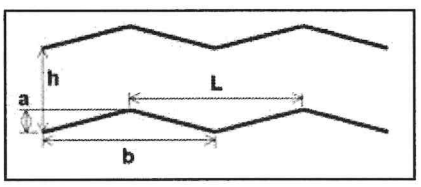

Figure 2. Schematic of the channel section geometry.

h	[mm]	10.00
a	[mm]	2.68
b	[mm]	20.00
L	[mm]	20.00
Vertex angle		150°
Channel width	[mm]	200.00
Hydraulic diameter	[mm]	18.18
Heigth to width ratio		0.05
Ribs number		30

Table 2. Channel geometric characteristics.

Velocity measurements are taken along the same lines at 20 points each.

From the temperature-gradient field we can reconstruct the heat flux field that can be displayed in a vector plot as shown in Figure 4 for the case of Re=1750; this kind of plot is impressive but gives essentially qualitative information like that heat flux on the wall is increasing while moving from the corrugation trough to the crest, or this increase is higher for the windward facet.

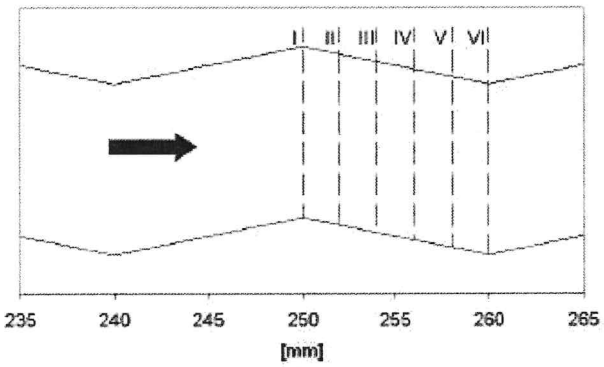

Figure 3. Traverse locations of heat flux measurement.

More details can be highlighted by plotting spatial trends of the x- and y-components of the temperature gradient. Figure 5 shows the values of the x-component of the temperature gradient measured along the first traverse for four different Reynolds numbers (y-axis origin falls on the apex of the thirteenth lower corrugation; the minus sign makes values concordant with heat-flux ones). Data display a decreasing trend, but with a quite flat region in the central zone of the traverse, which vanishes in the corrugation trough for every Reynolds number.

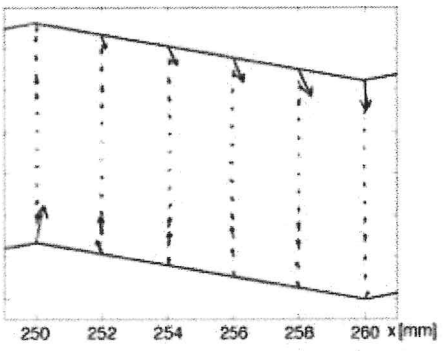

Figure 4. Heat flux vector plot for Re=1750.

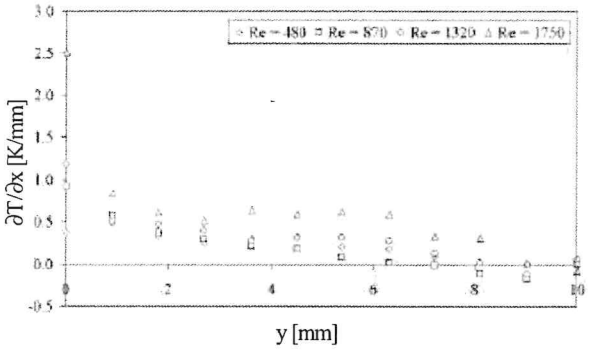

Figura 5. Temperature-gradient x-component.

Figure 6, instead, shows the distributions of the y-component of the temperature gradient along the sixth traverse for the same values Reynolds numbers of the previous figure; in this case, the y-axis origin falls on the bottom edge of the thirteenth lower corrugation. As it can be seen, trends for Re=480 and Re=870 are qualitatively similar between them, namely, a practically constant or slightly increasing piece with quite low values from the corrugation trough up near the middle of the channel and after a quasi-linear decreasing piece; finally, at the traverse upper end the temperature-gradient component attains its maximum value in module as this point falls on the corrugation apex.

At Re=1320, the curve modifies and data display larger variations between the corrugation trough and the middle of the channel; we conjecture they could be due to a lager recirculating region trapped inside the corrugations; moreover, near the upper wall the curve becomes more steep. Finally, the trend at Re=1750 is qualitatively similar to that at Re=1320, but fluctuations near the lower wall amplify and the slope near the upper wall is further increased.

The y-component of the temperature gradient was numerically integrated along the y-direction by means of the trapezoid method; imposing the measured value of the lower wall temperature, we reconstructed the temperature profiles along the six traverses. For instance, Figure 7 shows the reconstructed temperature profiles for Re = 1370; temperature is given in the non-dimensional form $\theta = (T - T_{in})/(T_w - T_{in})$ where T_{in} is the air temperature at the section inlet, and T_w the wall temperature; the θ-axis is parallel to the x-axis with a different origin for each traverse, taken in order that temperature profile starts from the point on the lower wall where traverse passes (worth noting temperature profile generally does not end in the corresponding point on the upper wall because of the experimental errors).

By inspection of the figure the following remarks can be evidenced. Profiles are asymmetric because heat fluxes at the lower and upper walls are different; the minimum is shifted toward the wall with higher thermal flux; the minimum value of heat flux is slightly increasing in the x-direction due to the bulk heating; finally, for Re=1750 temperature profile, not shown, looks more flattened because flow regime is becoming transitional.

The local Nusselt number distributions are shown in Figure 8; for a better understanding of the behavior along a corrugation module, the experimental points taken on the upper side are plotted translated of half a pitch, i.e., before that for the lower side, as if they had been obtained along the windward facet of the thirteenth lower corrugation.

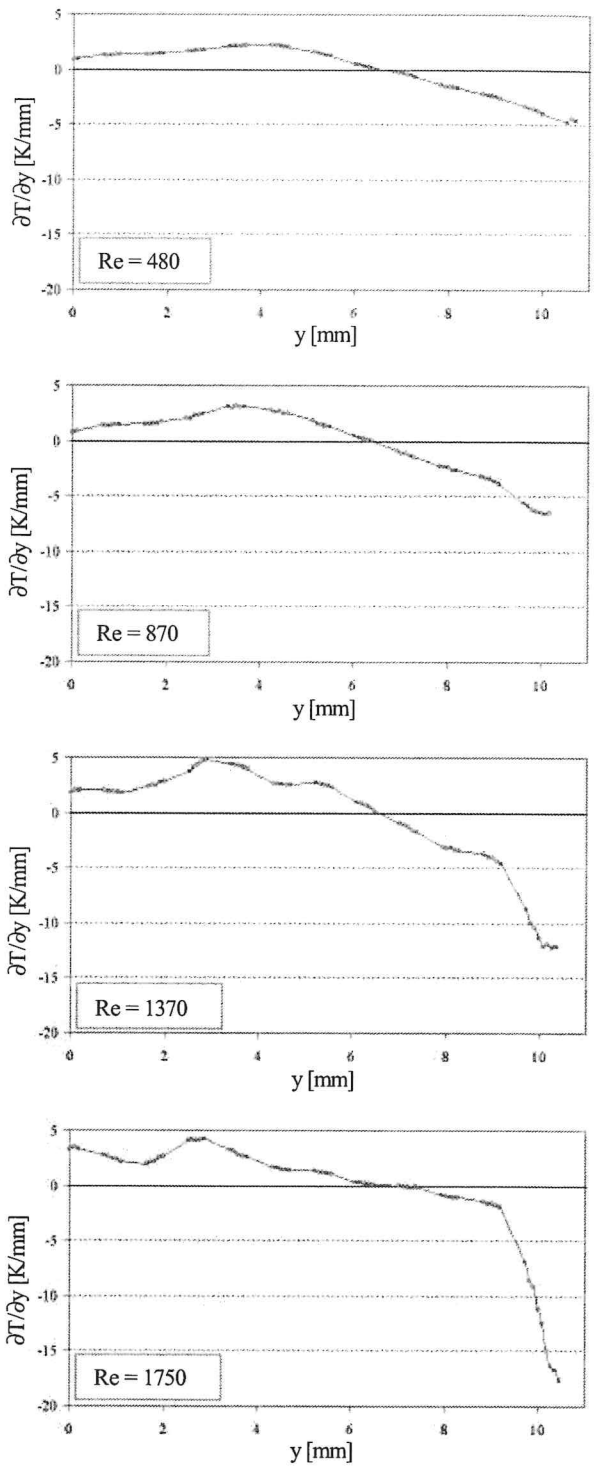

Figure 6. Temperature-gradient y-component.

This transposition is allowed for thermally fully developed flow and, in the present study, this assumption is supported by strong experimental indications. The distributions reported in Figure 8 are relative to four different Reynolds numbers, i.e., Re=480, Re=870, Re=1370 and Re = 1750. As it can be seen, the trends are quite similar between them; the local Nusselt number increases along the windward facet, it reaches a maxi-

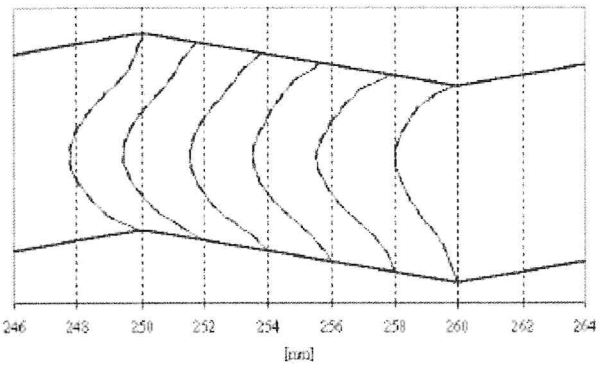

Figure 7. Temperature profiles for Re = 1370.

mum at the corrugation apex and from this point onwards it decreases at first very quickly and then more slowly, approaching the corrugation trough.

Maximum values, per-module mean values and a comparison with the plain channel are reported in Table 3.

In Figure 9 the average Nusselt number over the entire heated section is plotted versus the Reynolds number; for comparison, the figure also reports the values for a plain channel calculated by the correlations of Shah and London for Re≤2300, and of Gnielinsky for higher values [13]. As seen, for Re≤1370 flow regime is laminar and the average Nusselt number is practically a constant equal to 11.16, that is 67% higher than the plain-channel value; obviously, this value is also larger than the per-module average in the thermally fully developed region, because it benefits of the entry region. Consequently, waviness considerably alters the local convection coefficient distribution, but the average heat transfer increases to a less extent. In contrast, for Re>1370 the average Nusselt number starts to quickly increase, exhibiting a power-law dependence on the Reynolds number; up to Re=3100, the exponent is 1.43 and after it lowers to 0.8.

From this trend we argue the flow regime is transitional for Reynolds numbers between 1370 and 3100 and after it becomes fully turbulent. At Re=6300, corresponding to the upper limit of the investigated range, the average Nusselt number is nearly 80 with an over 400% increase with respect to the plain channel.

Finally, Figure 10 reports the experimental values of the apparent Darcy friction factor plotted versus the Reynolds number for the present channel and, for comparison, for a plain channel with the same width but 15 mm high. The friction factor for the wavy channel displays a trend similar to the plain channel in laminar flow regime but with 60% larger values; when the flow regime becomes transitional, the trend reverses and the friction factor starts to noticeably increase. As the Reynolds number is further increased, the growth attenuates and eventually, when flow is fully developed, the friction factor seems to attain the asymptotic value of 0.25 that is 7 times the plain channel value at Re=6300.

Re =	580	870	1320	1750
Nu_{max}	15.6	22.9	29.9	34.7
Nu_{av}	7.7	8.6	11.3	15.5
Nu_{plain}	6.6	6.6	6.6	6.6
Nu_{av}/Nu_{plain}	1.2	1.3	1.7	2.3

Table 3. Maximum and per-module mean values of the Nusselt number for the wavy channel.

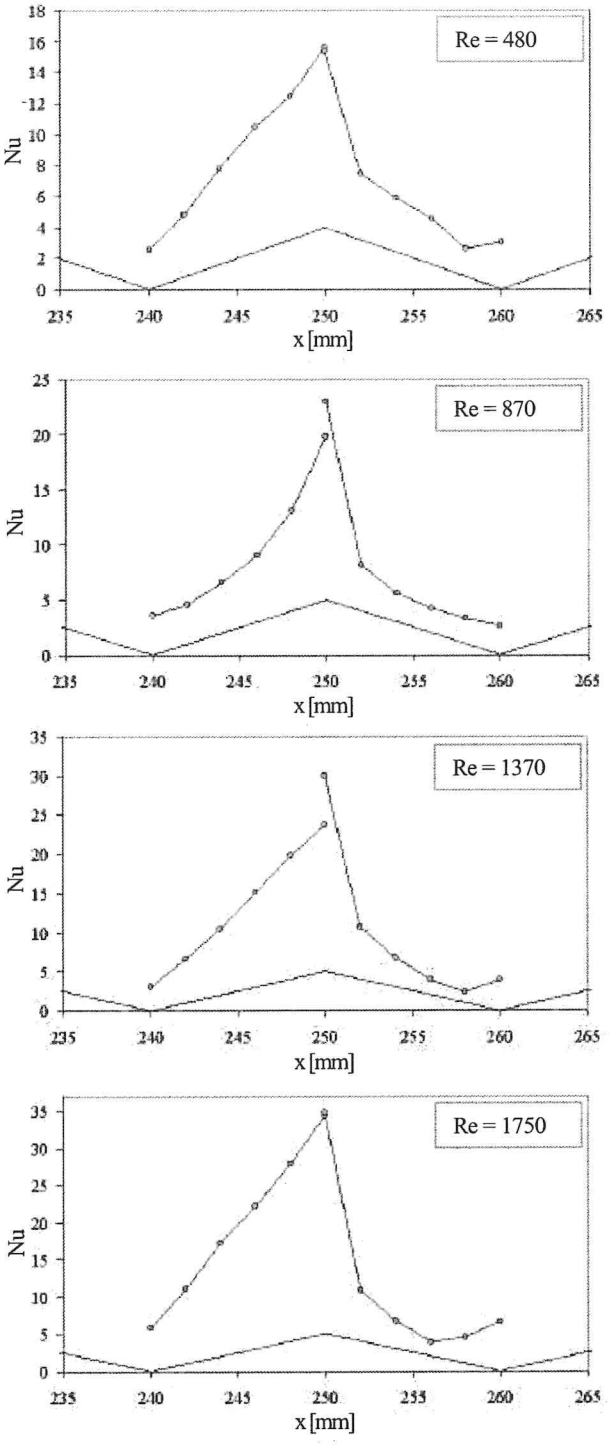

Figure 8. Local distributions of the Nusselt number.

CONCLUSIONS

This paper reports about an experimental investigation on heat transfer characteristics of an airflow inside a wavy channel at Reynolds numbers between 500 and 6300. The enhancement effect is essentially due to the periodic streamline deflection induced by the wall waviness. The heat transfer measurements over the entire channel show the flow is laminar up to Re=1370; within this regime, the average Nusselt

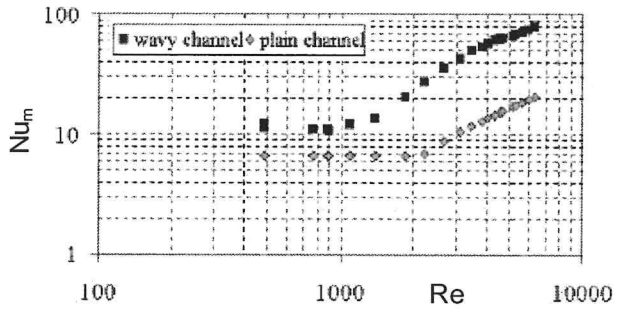

Figure 9. Average Nusselt number vs. Reynolds number.

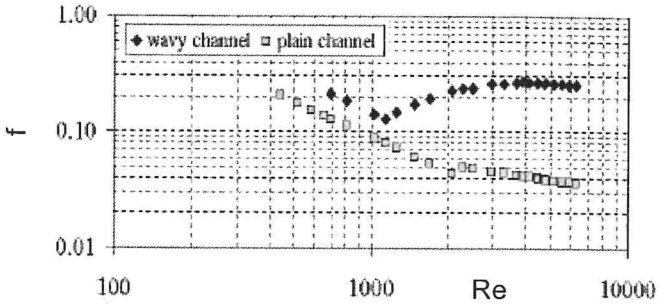

Figure 10. Apparent Darcy friction factor vs. Reynolds number.

number is independent of the Reynolds number, as for the flat-channel case, but its value is 67% higher; finally, local convection coefficient exhibits very far larger variations with respect to the plain-channel value.

In spite to these enhanced heat transfer characteristics, however, the Darcy apparent friction factor worsens of nearly 60%. At Re=1370, flow regime becomes transitional in advance, therefore, with respect to the plain channel. This event is well pointed out by a slope change in the average Nusselt number trend which from a constant becomes a power-law increasing function of the Reynolds number with an exponent of 1.43; the friction factor trend, however, does not exactly confirm this indication and suggests a slightly lower value of the Reynolds number for the occurrence of this regime. The transitional flow regime is characterized by a strong increase of the heat transfer coefficient and the apparent friction factor with respect to the plain-channel. Finally, for Re≥3100 flow becomes fully turbulent, the growth of the average Nusselt number with Re attenuates -the exponent of the letter lowers to 0.8, i.e., the characteristic value for plain channel-, and the apparent friction factor seems to asymptotically tend to 0.25. Consequently at Re=6300, i.e., the upper limit of the Re investigated range, the present wavy channel is characterized by an enhancement factor of 4 but with a 700% larger friction factor.

ACKNOWLEDGMENTS

This work is supported by MURST (the Italian Ministry for the University and for the Scientific and Technical Research) via COFIN 2002 grants.

REFERENCES

1. Fiebig, M., Vortices: tools to influence heat transfer. Recent developments, Proc. 2nd European Thermal Sciences and 14th UIT National Heat Transfer Conference, vol. 1 pp. 41-56, Rome, June 1996.
2. Webb, R.L., Principles of Enhanced Heat Transfer, John Wiley & Sons, cap. 9, pp. 228-284, 1994.
3. Kays, W.M., Compact Heat Exchangers, AGARD Lecture Ser. No. 57 on Heat Exchangers, ed. Gnoux, AGARD-LS-57-72, Jan. 1972.
4. Joshi, H.M., Webb, R.L., Prediction of heat transfer and friction in the offset strip fin array, Int. Journal of Heat and Mass Transfer, Vol. 30, No. 1, pp. 69-84, 1987.
5. Wieting, A.R., Empirical correlations for heat transfer and flow friction characteristics of rectangular offset fin heat exchangers, J. Heat Transfer, Vol. 97, pp. 488-490, 1975.
6. Davenport, C.J., Correlations for heat transfer and flow friction characteristics of louvered fin, Heat transfer-Seattle 1983, AIChE Symp. Ser., No. 225, Vol. 79, pp. 19-27, 1984.
7. Goldstein, L.J., Sparrow, E.M., Heat/mass transfer characteristics for flow in a corrugated wall channel, J. Heat Transfer, Vol. 99, pp. 187-195, 1977.
8. Ali, M.M., Ramadhyani, S., Experiments on convective heat transfer in corrugated channels, Experimental Heat Transfer, Vol. 5, pp. 175-193, 1992.
9. Fomin N.A., Speckle photography for fluid mechanics measurements, Berlin, Springer, 1998.
10. Jones R., Wykes C., Holographic and Speckle Interferometry, Cambridge University Press, 1983.
11. Curotti A., Ia fotografia speckle digitale nell'analisi dei campi termici, Tesi di Dottorato di Ricerca XII ciclo, Politecnico di Milano, 1999.
12. Colombo, L., Muzzio, A., Niro, A.,"Experimental results on convective heat transfer of an air-flow through a wavy channel". Proc. 4th European Thermal Sciences Conference, Session 7&10 ENH, Birmingham, 2004.
13. Kakaç S., Shah R. K., Win A., Handbook of Single-Phase Convective Heat Transfer, John Wiley & Sons, New York, 1987.